Available online at www.sciencedirect.com
ScienceDirect
Journal of the European Ceramic Society 32 (2012) 399–408
www.elsevier.com/locate/jeurceramsoc

Porous wollastonite–hydroxyapatite bioceramics from a preceramic polymer and micro- or nano-sized fillers

Enrico Bernardo [a,*], Paolo Colombo [a,e], Ilaria Cacciotti [b], Alessandra Bianco [b], Rossella Bedini [c], Raffaella Pecci [c], Karoline Pardun [d], Laura Treccani [d], Kurosch Rezwan [d]

[a] *Dipartimento di Ingegneria Meccanica, University of Padova, Italy*
[b] *Dipartimento di Scienze e Tecnologie Chimiche, INSTM UdR Roma Tor Vergata, University of Rome "Tor Vergata", Italy*
[c] *Technology and Health Department, Italian National Institute of Health, Rome, Italy*
[d] *Advanced Ceramics Group, Faculty of Production Engineering, University of Bremen, Germany*

Received 3 March 2011; received in revised form 5 August 2011; accepted 7 August 2011
Available online 7 September 2011

Abstract

Wollastonite–hydroxyapatite ceramics have been successfully prepared by a novel method, corresponding to the thermal treatment in air of a silicone embedding micro- and nano-sized fillers. $CaCO_3$ nano-sized particles, providing CaO upon decomposition, acted as "active" filler, whereas different commercially available or synthesised hydroxyapatite particles were used as "passive" filler. The homogeneous distribution of CaO, at a quasi-molecular level, favoured the reaction with silica derived from the polymer, at only 900 °C, preventing extensive decomposition of hydroxyapatite. Open-celled porous ceramics suitable for scaffolds for bone–tissue engineering applications were easily prepared from filler-containing silicone resin mixed with sacrificial PMMA microbeads as templates. The pore size (in the range of 80–400 μm) and the open porosity percentage (40–50%) were evaluated by means of micro-computerized tomographic analysis. A preliminary assessment of the biocompatibility and cell activity of the produced ceramics was performed successfully by *in vitro* tests using human osteoblast cells.

Keywords: A. Precursors; B. Nanocomposites; D. Apatite; D. Silicate; E. Biomedical applications

1. Introduction

Silicone resins represent the most investigated type of preceramic polymers, i.e. polymers that are subjected to conversion into ceramics upon heat treatment. The fundamental advantage of these polymers is the possibility of combining shaping and synthesis of ceramics, in a very easy way: components may be shaped by conventional plastic-forming techniques, such as spinning, blowing, injection molding, warm pressing, resin transfer molding, applied to the precursor polymers, and later converted into ceramics (generally named "polymer-derived ceramics", or PDCs, in order to emphasize their origin) by treatments above 800 °C.[1,2]

As demonstrated by recent investigations about mullite ($3Al_2O_3{\cdot}2SiO_2$), mullite matrix composites, and SiAlONs, silicones have the potential of yielding widely used engineering ceramics, when filled with oxide nano-particles, maintaining their processing advantages.[3–7] Silicones act as sources for silica, which reacts easily with the nano-sized inclusions due to the quasi molecular mixing provided by the precursors. In fact, the mixing with the filler is greatly favoured by the fact that silicones are easily dissolved in common solvents, such as acetone or isopropyl alcohol, leading to solutions in which nano-particles can be put in suspension. The drying of such a suspension gives a nano-composite solid residue, easily ground into fine powders for the final shaping (by cold or warm pressing) of the preceramic body. The usage of filled silicones in the combined shaping and synthesis of silicates is of undoubted interest, since these compounds are known to possess a high thermal and chemical

* Corresponding author. Fax: +39 049 8275505.
E-mail address: enrico.bernardo@unipd.it (E. Bernardo).
[e] Also in Department of Materials Science and Engineering, The Pennsylvania State University, University Park, Pennsylvania 16801, United States.

0955-2219/$ – see front matter © 2011 Elsevier Ltd. All rights reserved.
doi:10.1016/j.jeurceramsoc.2011.08.010

stability but also to exhibit a poor solid state sinterability, due to their partially covalent bonding.[8]

The present paper was conceived to study the feasibility of bioceramics based on wollastonite (calcium mono-silicate, $CaO{\cdot}SiO_2$), from silicones with appropriate "active" and "passive" fillers. The application of silicones to the manufacturing of calcium silicate ceramics has been scarcely investigated in literature.[9–11] Although effective in yielding wollastonite, the previous papers have evidenced a poor control of phase purity; in particular, the combination of a silicone resin with several CaO precursors, such as $CaCO_3$ micro-particles, Ca-acetate and CaO nano-particles, "active" in reacting with the silica-rich residue of the polymer, led to a number of secondary phases, after treatments at 1000–1200 °C in nitrogen.[11] The present investigation shows the obtainment of almost pure wollastonite from a silicone resin containing $CaCO_3$, in the form of micro- or nano-sized particles, after treatment at only 900 °C in air. The obtainment of wollastonite–hydroxyapatite composites was optimized by the insertion of hydroxyapatite (HAp, $Ca_{10}(PO_4)_6(OH)_2$) particles as "passive" fillers, together with $CaCO_3$ active filler. In this case, unlike most situations described in the literature, the passive fillers were added not only to control the shrinkage, by simply diluting the transforming mass,[12] but also to provide a specific functionality, obtaining the typical phase assemblage of one of the most studied glass–ceramics, widely used for load-bearing implants.[13,14] In fact, it is well known that among calcium phosphate compounds, HAp is the most employed material in hard tissue implants and bone–tissue engineering applications, due to its similarity to the bone inorganic component, excellent biocompatibility and osteoconductivity.[15] Several formulations demonstrated a promising biocompatibility and bioactivity, together with their suitability for the manufacturing of strong, open-celled porous ceramics, to be used in bone replacement and restoration applications.

2. Experimental procedure

2.1. Materials Preparation

A commercial silicone resin (polysilsesquioxane Silres® MK, Wacker-Chemie GmbH, Munich, Germany, later referred to simply as "MK") was dissolved in isopropanol and mixed, firstly, with only one type of filler, consisting of nano-sized $CaCO_3$ powders (average diameter of $d_{50} = 90$ nm, specific surface of 20 m^2/g, PlasmaChem GmbH, Berlin, Germany). The mixing was performed under magnetic stirring, followed by ultrasonication for 10 min, which allow to obtain stable and homogeneous dispersions. For comparison purposes, mixtures with micro-sized $CaCO_3$ (average diameter of 10 μm, Sigma–Aldrich Ltd, Gillingham, UK) were also prepared. The $CaCO_3$/MK silicone weight ratio was kept constant and equal to 1.4. Further mixtures were similarly prepared by adding both nano-sized $CaCO_3$ powders and hydroxyapatite powders, in the form of commercially available powders, micro- (HAp M, P260 S, Plasma Biotal Ltd, Tideswell, UK, $d_{50} = 3$ μm) and nano-sized (HAp C, Centro Ricerche Colorobbia, Vinci, Italy, $d_{50} < 100$ nm), and of laboratory-prepared nano-sized elongated particles (HAp I), as reported elsewhere.[15] Briefly, the HAp I powders were synthesized by titration of 10 g/l aqueous suspension of calcium hydroxide ($Ca(OH)_2$, Sigma–Aldrich, Gillingham, UK, purity 99.5%, MW 74.10) with a phosphoric acid solution (H_3PO_4, Sigma–Aldrich, purity 86.3%, MW 98.00). The pH was finally adjusted to 9.4. Precipitates were aged in mother liquor at room temperature, washed with NH_4OH aqueous solution, vacuum filtered and finally dried at 60 °C. The obtained powders consisted in monophasic hydroxyapatite, thermally stable up to 1300 °C, composed of nano-sized, needle-like particles (10–20 nm wide and 50–200 nm long), featuring a specific surface area of 80 m^2/g.[16,17]

The amount of HAp powders was kept equal to the theoretical solid residue of the reaction between $CaCO_3$ and silicone.

The materials obtained after drying the dispersions in an oven in air at 60 °C overnight were ground into fine powders by pestle and mortar and cold-pressed in a cylindrical steel die applying a pressure of 40 MPa for 2 min, without using any binder. Disc specimens with a diameter of 30 mm and thickness of approximately 2 mm were obtained and heat treated at 900 °C for 1 h; the heating rate was 2 °C/min, except in the interval 500–700 °C, in which it was fixed at 0.5 °C/min.

Powders of silicone resin embedding the fillers, with selected formulations, were also mixed with PMMA micro-beads (Cray Valley Waterborne Polymers Department, Atofina Italia, Milan, Italy), having an average dimension of 500 μm, in a concentration of 40–45 wt%, following a procedure similar to that employed for silicon oxycarbide (SiOC) microcellular foams.[18,19] After dry ball mixing for 30 min, the powders were warm pressed at 170 °C, under a pressure of 20 MPa, into discs with a diameter of 50 mm and a height of 9 mm. Successively, the obtained specimens were pre-treated in oxidative atmosphere at 270 °C (with a heating rate of 0.5 °C/min), for burning out the PMMA microbeads, and the resulting cellular materials were subjected to the same thermal treatment reported above.

2.2. Microstructural characterization

The density of discs and foams was determined geometrically and by weighing using a digital balance. The true density of the various samples was measured by means of a gas pycnometer (Micromeritics AccuPyc 1330, Norcross, GA), operating with He gas on samples in powdered form. Compositional and microstructural characterizations were performed by optical stereomicroscopy and scanning electron microscopy (FEI Quanta 200 ESEM, Eindhoven, The Netherlands) equipped with EDS.

Micro-computerized tomography (microCT) was used for a non-destructive evaluation of the three-dimensional (3D) porosity and pores interconnectivity of the produced foams. Selected samples were scanned with a SkyScan 1072 microCT imaging system (Kontich, Belgium) at 12.7 μm resolution, using a voltage of 100 kV, and a current of 98 μA. The data sets were acquired over a rotation range of 180° (with

0.45° rotation step) and reconstructed with software (Cone_Rec v2.23; Skyscan) to calculate morphometric parameter (CTAnalyser v1.11; Skyscan) and to build the 3D models (ANT 3D Creator, v2.4; Skyscan). Image reconstruction and analysis were conducted using the software package provided by SkyScan. In details, the raw images of samples were first reconstructed to serial coronal-oriented tomograms using a 3D cone beam reconstruction algorithm. Then, representative 3D reconstructions of porous foams were generated based on the binarized tomograms to visually show the 3D models of sample structures. Sample porosity was then calculated as:

$$\text{Porosity} = 100\% - \text{vol\% of binarized object}$$

(scaffold materials) in Volume Of Interest (VOI)

The average diameter was calculated considering three different slices for sample and carrying out the measurements on 30–40 selected pores for each slice by means of *Image J* (*NIH*) software. The interconnectivity evaluation was carried out on the 3D reconstructions using the 'shrink-wrap' function, which allows measuring the pore volume fraction in a scaffold that is accessible from the outside through openings of a certain minimum size.[20] According to this algorithm, spheres are ideally placed inside the cells: if spheres touch with each other, the interconnectivity is 100%. A shrink-wrap process was performed between two 3D measurements to shrink the outside boundary of the VOI in a scaffold through any openings whose size is equal to or larger than a threshold value (50–300 μm in this study). Interconnectivity was calculated as follows:

$$\text{Interconnectivity} = \frac{(V - V_{\text{shrink-wrap}})}{(V - V_m)} \times 100\%$$

where V is the total volume of VOI, $V_{\text{shrink-wrap}}$ is the volume after shrink-wrap processing, and V_m is the volume of scaffold material.[20]

The phase identification was performed by means of X-ray diffraction (XRD; Bruker AXS D8 Advance, Bruker, Germany), supported by data from PDF-2 database (ICDD-International Centre for Diffraction Data, Newtown Square, PA). Rietveld's refinement was applied to all XRD patterns by means of the MAUD software package,[21] and convergence was reached in the refinement of all patterns. From the refinement analysis it was possible to obtain a semi-quantitative estimation of the volume fraction and crystal size of different phases. The crushing strength of the foams was measured by compression testing at room temperature, using an Instron 1121 UTM (Instron Danvers, MA, equipped with a 10 kN load cell) with a cross-head speed of 1 mm/min, on samples of a nominal size of 5 mm × 5 mm × 10 mm, cut from larger specimens. Each data point represents the average value of 5–10 individual tests.

2.3. Preliminary biological tests

Preliminary biological tests were conducted on composites comprising HAp I filler, in the form of small tiles (10 mm × 10 mm × 1.5 mm) cut from discs obtained by simple cold pressing and subsequent thermal treatment.

Human osteoblast cells (HOB) (passage 4, Provitro GmbH, Berlin, Germany) were cultured in Dulbecco/Vogt modified Eagle's minimal essential medium (D-MEM, high glucose, Gibco, Invitrogen GmbH, Darmstadt, Germany) supplemented with 10% heat-inactivated fetal calf serum (FCS, Sigma–Aldrich, Germany) and 1% antibiotic–antimycotic (Invitrogen, Germany) in an incubator (C200, Labotect Labor-Technik-Göttingen GmbH, Göttingen, Germany) at 37 °C, 10% CO_2 and 95% RH. The ceramic samples were sterilized by a 30 min UV-light treatment on each side, afterwards placed in 24-well multidishes and rinsed two times with cell medium. Osteoblasts were seeded onto the ceramic samples at a density of 4×10^4 cells/mL. The cell culture medium was changed every 2 days. Nunc Thermanox® coverslips (Thermo Fisher Scientific Inc., Bonn, Germany), of 15 mm diameter, were used as a reference material.

The viability of the HOBs was determined by a water-soluble tetrazolium salt (WST-1) assay (Roche Diagnostics GmbH, Penzberg, Germany). The WST assay used is based on the reductive cleavage of WST-1 by mitochondrial dehydrogenase to soluble formazan, which is active only in viable cells. At days 4 and 10 of culture 100 μL WST-1 reagent was added to the culture wells and incubated for 3.5 h at 37 °C, 10% CO_2 and 95% RH. The level of dye formed was then measured immediately using a microplate reader (Chameleon, HIDEX, Turku, Finland) at 450 nm and a reference wavelength of 650 nm.

After 4 and 10 days of culture, cells were rinsed twice with phosphate buffered saline (PBS; Sigma–Aldrich) and fixed in 4% paraformaldehyde (PFA) (Honeywell Riedel-de Haën, Seelze, Germany) for 15 min at 37 °C. After rinsing with PBS, cells were permeabilized for 3 min with 0.5% Triton-X (Sigma–Aldrich). All samples were incubated with a mixture of 4,6-diamidino-2-phenylindole (DAPI) (0.5 μg/mL, Sigma–Aldrich) and AlexaFluor®488 Phalloidin (2 U/mL, Invitrogen) for 45 min at room temperature in the dark. After additional washing steps with PBS and PFA the cells were visualized using AxioVision Microscope Imager M.1 (Carl Zeiss AG, Jena, Germany).

As a reference, the samples were soaked in cell culture medium (CCM), without the presence of cells, under static conditions. The samples were immersed in 25 mL CCM in clean conical flasks at pH 7.40 and 37 °C for 7 days. CCM consisted of Minimum Essential Medium Eagle (Sigma–Aldrich) supplemented with 10% FCS (Sigma–Aldrich), 1% antibiotic–antimycotic (Invitrogen), 10 mM β-glycerol phosphate (Sigma–Aldrich), 50 μg/mL sodium L-ascorbate (Sigma–Aldrich) and 10^{-8} M dexamethasone (Sigma–Aldrich). After 7 days, the samples were removed from the CCM, gently washed with deionised water and dried at 40 °C. After drying, the surface of the samples was examined by scanning electron microscopy (SEM, Cambridge Instruments, Cambridge, UK) and by Energy Dispersive Spectroscopy (EDS, Camscan Series 2, Obducat CamScan Ltd., Cambridge, UK).

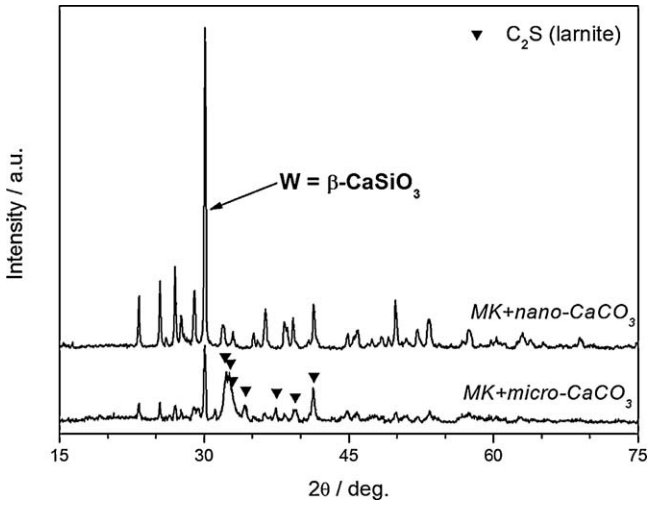

Fig. 1. Comparison between the ceramic residue (after treatment at 900 °C in air) of MK silicone resin/micro-$CaCO_3$ mixture and that of MK silicone resin/nano-$CaCO_3$: all non-indexed peaks correspond to β-wollastonite.

3. Results and discussion

The chosen $CaCO_3$/MK silicone weight ratio was considered on the basis of previous experiments with MK and precursors of CaO, described by Bernardo et al.[11] Those experiments, although conducted in N_2 atmosphere, instead of air as in the present case, highlighted that wollastonite was hardly the only phase developed, even in the presence of a CaO/SiO_2 molar ratio equal to 1, effectively corresponding to $CaO{\cdot}SiO_2$ (Ca monosilicate or C·S). In fact, obtained data indicated that wollastonite was accompanied by secondary silicates (in polymorphic forms) corresponding to a CaO/SiO_2 molar ratio > 1, such as rankinite, $3CaO{\cdot}2SiO_2$ ($C_3{\cdot}S_2$), di-calcium silicate, $2CaO{\cdot}SiO_2$ ($C_2{\cdot}S$), tri-calcium silicate $3CaO{\cdot}SiO_2$ ($C_3{\cdot}S$), etc. These secondary phases were attributed to local fluctuations in the CaO/SiO_2 molar ratio, due to an inhomogeneous distribution of CaO, from the various precursors.

With the present filler/silicone ratio (1.4), owing to the CaO yield of $CaCO_3$ (56%) and the silica yield of MK (84%), the actual CaO/SiO_2 molar ratio was slightly lower than 1 (1.4·0.56/0.84 = 0.94). This choice was conceived in order to favour the formation of the monosilicate (i.e. wollastonite), since even upon higher local concentrations of CaO, the molar ratio of constituent oxides would be close to the desired one. Fig. 1 indeed shows that, using a micro-$CaCO_3$ filler, it was possible to obtain, for a treatment in air at 900 °C, a significant formation of wollastonite in its β form (PDF #76-0186, the un-labelled peaks in the figure are all attributable to this phase). However, di-calcium silicate in its β form, i.e. β-$C_2{\cdot}S$ or larnite (PDF #33-302), was still present. From Rietveld's refinements, the crystallinity was estimated to be about 80%, with $C_2{\cdot}S$ representing the main phase in an amount of 58 wt%. This is likely due to the fact that local high concentrations of CaO, associated to the micrometric size of filler, were present, and the silica from the silicone resin did not react completely with the calcium oxide, giving rise to an amorphous silicate phase. In any case, the improvement in the yield of calcium silicates, compared to previous experiences, is particularly significant: in N_2 atmosphere, with a CaO/SiO_2 molar ratio equal to 1, the crystallinity at 1000 °C was below 70 wt%, with β-wollastonite representing no more than 10% of the total amount of crystals.[11] While in the experiments in N_2 atmosphere high crystallinities were achieved above 1000 °C, with a significant formation of α-wollastonite, the present treatments in air practically give origin only to β-wollastonite. Further studies will be undoubtedly needed, but this behaviour is likely associated to differences in molecular structure of the solid residues of MK resin with varying atmosphere of ceramic conversion.

The use of $CaCO_3$ nano-sized particles, rather than micro-sized ones, was particularly effective in changing the product of MK/CaO interaction, as shown by the same Fig. 1. The Rietveld's refinements revealed that nano-particles led to a ceramic with a very high crystallinity (∼97%) and wollastonite as the main phase (∼88%). The increase in crystallinity is reasonably attributable to the superior reactivity of nano-sized fillers, as already observed for mullite ceramics.[3,4] The much reduced formation of $C_2{\cdot}S$ is in turn likely due to the more homogeneous distribution of CaO within the preceramic polymer, deriving from the decomposition of the nano-filler, in comparison to that obtainable with the micro-sized filler previously tested.[11] The crystal size of both wollastonite and $C_2{\cdot}S$ was estimated to be in the order of 100 nm. It is interesting to note again a substantial improvement, compared to previous experiments in nitrogen atmosphere, in which high yields of wollastonite (in its α-form) were achieved above 1000 °C with a Ca acetate aqueous solution, after a complicated mixing with a solution of MK polymer, or with CaO nano-particles, difficult to be handled, due to the easy reaction with moisture. The improvement does not concern only the phase assemblage and the processing temperature, but also the possibilities of extensive application of the present approach, since nano-sized $CaCO_3$ is known to be available as commercial product for the industrial filling of common plastics and rubbers.[22,23]

The discs obtained from MK silicone and $CaCO_3$, treated at 900 °C, although featuring the desired phase, contained numerous cracks. The cracking of samples was expected, due to the release of gas from both polymer-to-ceramic conversion of the silicone and from decomposition of the carbonate. More mechanically resistant materials, although porous, were produced by inserting a secondary, "passive" filler, i.e. hydroxyapatite powders, which reduced the shrinkage and provided a pathway for the release of the gaseous species during heat treatment. The introduction of this specific phase was aimed at reproducing, in a polymer-derived-ceramic, the coupling of wollastonite and hydroxyapatite, present in the well known silico-phosphate glass–ceramics for biomedical applications.[13]

Fig. 2 illustrates a comparison between ceramics obtained by using different types of hydroxyapatite filler. It may be observed that with micro-sized HAp powders (HAp M) only the desired phases, i.e. wollastonite and hydroxyapatite, are present. Both phases, in fact, exhibit well defined diffraction peaks. When using nano-sized HAp powders (HAp I and HAp C), the diffraction patterns of the ceramized samples appear to be quite different; the peaks associated to HAp are much

Table 1
Phase balance and crystal size in wollastonite–hydroxyapatite composites.

Formulation: MK/nano-$CaCO_3$ +...	Phase content (wt%) [crystal size]			
	HAp	Wollastonite (W)	Dicalcium silicate (C_2·S)	Amorphous phase
HAp M (micro-powders)	35 [3 μm]	35 [120 nm]	0	30
HAp C (nano-powders)	30 [160 nm]	18 [80 nm]	28 [100 nm]	24
HAp I (nano-powders)	40 [200 nm]	18 [100 nm]	22 [100 nm]	20

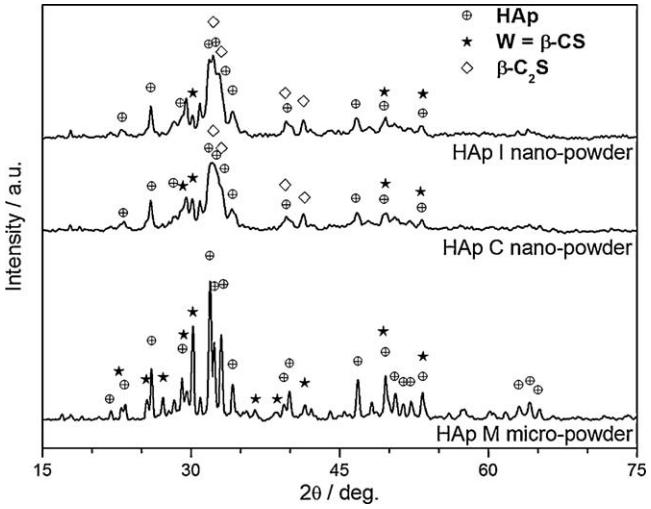

Fig. 2. Comparison between different wollastonite–hydroxyapatite composites, developed from different hydroxyapatite fillers, after thermal treatment in air at 900 °C.

broader, due to the nanometric size of the crystals, and a secondary calcium silicate is present besides wollastonite. As in the case of samples from simple MK/$CaCO_3$ micro-powders, the secondary calcium silicate corresponds to C_2·S. This phase formed because of a local high concentration of CaO, likely associated to the partial decomposition of HAp nano-particles. The Rietveld's refinements allowed a quantification of both phase balance and crystal size, as reported in Table 1. In all composites, some HAp decomposition indeed occurred, since the weight content of this phase is lower than the expected on the basis of the MK/$CaCO_3$/HAp formulations, which was aimed at forming ceramics with a 50/50 wt ratio between wollastonite and hydroxyapatite. HAp I powders (nano-sized hydroxyapatite) displayed a higher phase stability with respect to commercially available nano-sized powders (HAp C), confirming previous results.[16,17] The data for the sample produced using micro-sized HAp (HAp M) confirmed that wollastonite was the only calcium silicate phase formed, leading also to a composite ceramic comprising the highest content of amorphous phase. The calcium silicate phases developed in the form of sub-micron crystals, i.e. with a crystal size around 100 nm, as reported in Table 1.

The formulations for wollastonite–hydroxyapatite composites were employed for the preparation of highly porous, cellular materials. Although not corresponding to the perfect mixing of the desired phases, the produced ceramic composites featured a phase balance effectively resembling that of wollastonite/apatite glass–ceramics for biomedical applications, i.e. an almost equal content of silicate and phosphate crystal phases, with ~30 wt% of amorphous phase.[13] The use of a preceramic polymer gave the opportunity to employ techniques for the production of ceramic foams, such as the use of sacrificial templates, which are not easily applicable to glass–ceramics, leading to highly homogeneous open-cell structures. It should be noted, however, that part of the porosity is generated by the gases released from the decomposition of the calcium carbonate.

Table 2 summarizes the physical and mechanical properties of foams developed by means of PMMA microbeads using mixtures containing different types of secondary HAp fillers. Despite the remarkable amount of porosity developed, always exceeding 70 vol%, some samples possessed a very high crushing strength. In particular, the sample containing HAp C filler, exhibited a crushing strength comparable to that of natural trabecular bone, which hardly exceeds 10 MPa.[24]

The lower mechanical strength of foams containing HAp I powders can be explained considering that these samples, as shown in Fig. 3a, presented a higher porosity and a less homogeneous microstructure, in comparison to those containing other HAp fillers, as shown in Fig. 3b and c. In particular, the circles in Fig. 3a evidence that quite large, porous struts exist around the main cells. It is well known that nano-sized fillers greatly enhance the viscosity of the polymer matrices in which they are embedded[25]: the increased viscosity resulted in a limited flow of the silicone resin within the PMMA templates upon warm pressing. HAp I powders are more critical in this respect, since

Table 2
Physical and mechanical properties of produced wollastonite–hydroxyapatite foams.

Formulation: MK/nano-$CaCO_3$ +...	PMMA content (wt%)	Density (g/cm^3)	Total porosity (vol%)	Crushing strength (MPa)
HAp M (micro-powders)	45	0.73 ± 0.06	78	5.3 ± 1.5
HAp C (nano-powders)	40	0.90 ± 0.03	72	7.8 ± 1.8
	45	0.82 ± 0.03	75	3.4 ± 1.6
HAp I (nano-powders)	40	0.66 ± 0.04	80	1.7 ± 0.6
	45	0.61 ± 0.04	82	1.6 ± 0.7

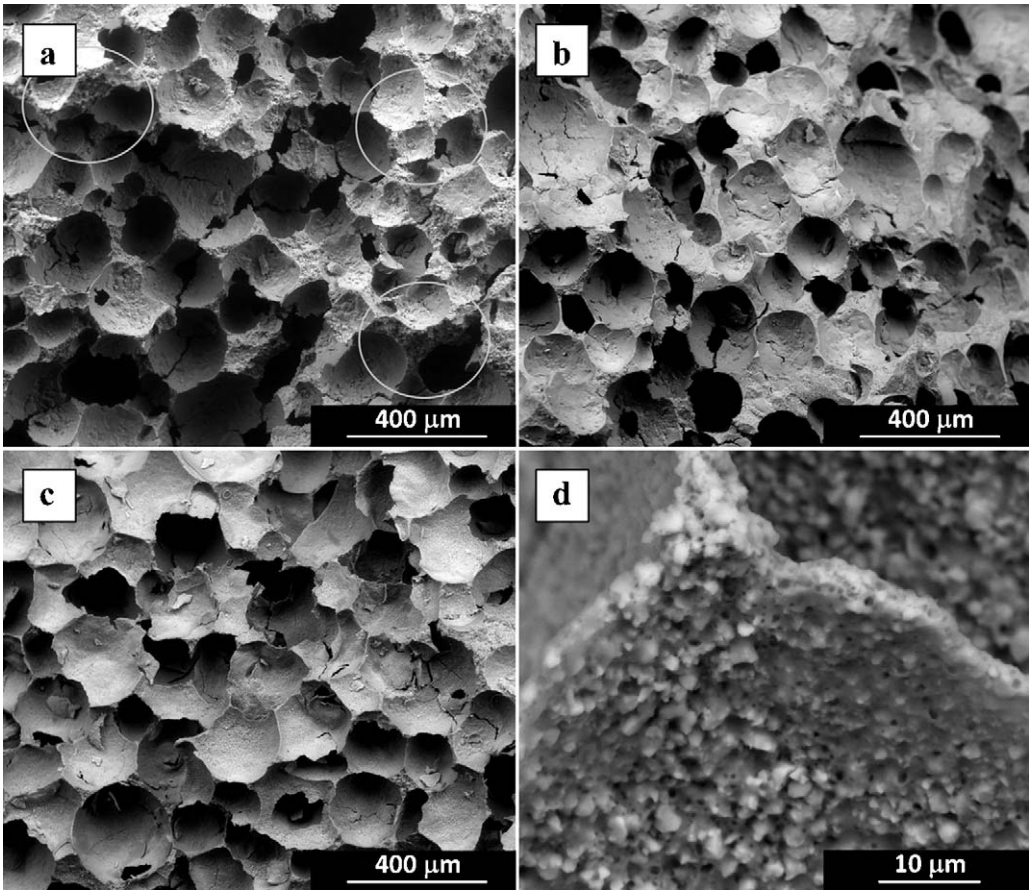

Fig. 3. Microstructure of wollastonite–hydroxyapatite foams from MK, nano-$CaCO_3$ and: (a) HAp I nano-powders (circles underline porous struts); (b) HAp C nano-powders; (c and d) HAp M micro-powders.

they combine the nanometric size with an elongated morphology, also known to provide a significant increase of viscosity in a fluid.[26] Moreover, the HAp I particles were as-precipitated and not subjected to a thermal pretreatment, whereas the commercial powders were typically treated at high temperature. Thus it could be possible that relevant weight losses occurred during the densification process with a detrimental effect on the mechanical properties.

Fig. 3d provides a high magnification detail for a foam produced from HAp M micro-powders (already shown in Fig. 3c). It may be noted that the sample exhibits a hierarchical porosity: besides larger pores (cells deriving from the elimination of the PMMA templates, with a diameter of several hundred microns), there is a number of micropores in the cell walls. The presence of these micropores is attributable to the gas evolution occurring with the decomposition of nano-sized $CaCO_3$. In fact, $CaCO_3$ decomposes in a temperature range which overlaps with the beginning of polymer-to-ceramic conversion of the silicone.[2] The strength measured for the foam from HAp M is remarkable, especially if we consider the porosity of the struts, which normally has a weakening effect on ceramic foams.[27] Moreover, the combination of microporosity and roughness, associated to the formation of microcrystals (also evident in the cell walls), undoubtedly provides a high amount of geometric surface, that could be exploited, in the view of biomedical applications, for drug impregnation or improved cell adhesion and proliferation.[28]

Micro-tomography, applied on selected samples, was useful to investigate the pores distribution and to evaluate the interconnectivity. In Fig. 4a and b, as an example, the three-dimensional structure reconstructions, by convolution of multiple scans (*Ctan software*), of samples HAp C (45% PMMA) and HAp I (45% PMMA) are compared. The calculated morphometric parameters are collected in Table 3. It was observed that the pore diameters ranged from 75 to about 400 μm, i.e. very close to the widely considered optimal range (100–300 μm) for bone ingrowth.[29,30] However, there is a significant discrepancy between the porosity measured by micro-tomography and that from density measurement. It has to be pointed out that the significant discrepancy between porosity as evaluated by micro-tomography and as calculated by means of density measurement has to be associated to the presence of microporosity, considering that the minimum resolution of micro-CT is around 5 μm. According to Sanchez-Salcedo et al.,[31] microporosity might play an active role in term of type of attracted cells, cellular development, orientation and directionality of cellular ingrowth. It is interesting to note that the difference is much larger for the sample produced starting from the HAp I filler than from the HAp C one. In our opinion this fact could be seen as a confirmation of the higher difficulties in viscous flow of the

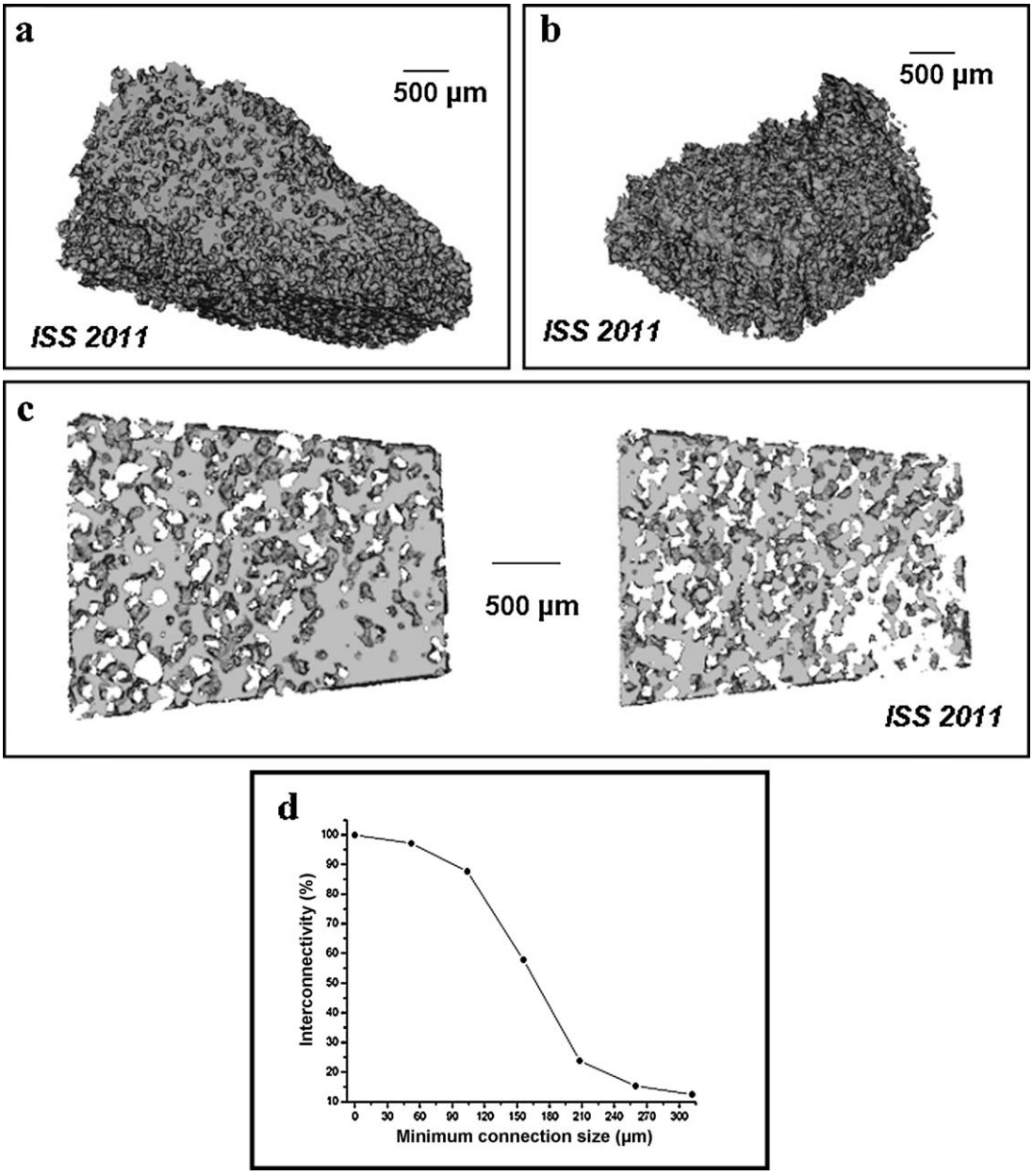

Fig. 4. X-ray micro-computed tomography results: three-dimensional model of sample with HAp I, 45% PMMA (a) three-dimensional model; (b) selected sections; (c) and interconnectivity vs minimum connection size; (d) for sample with HAp C, 45% PMMA.

Table 3
Morphometric parameters obtained from micro-tomographic analysis.

Sample	MK/nano-$CaCO_3$ +...			
	HAp C (nano-powders) 40% PMMA	HAp C (nano-powders) 45% PMMA	HAp I (nano-powders) 40% PMMA	HAp I (nano-powders) 45% PMMA
Porosity (%)	44	50	40	43
Minimum pore diameter (μm)	75 ± 3	80 ± 3	90 ± 4	175 ± 3
Maximum pore diameter (μm)	345 ± 4	390 ± 6	381 ± 3	330 ± 5
Average pore diameter (μm)	165 ± 50	165 ± 65	170 ± 65	190 ± 60

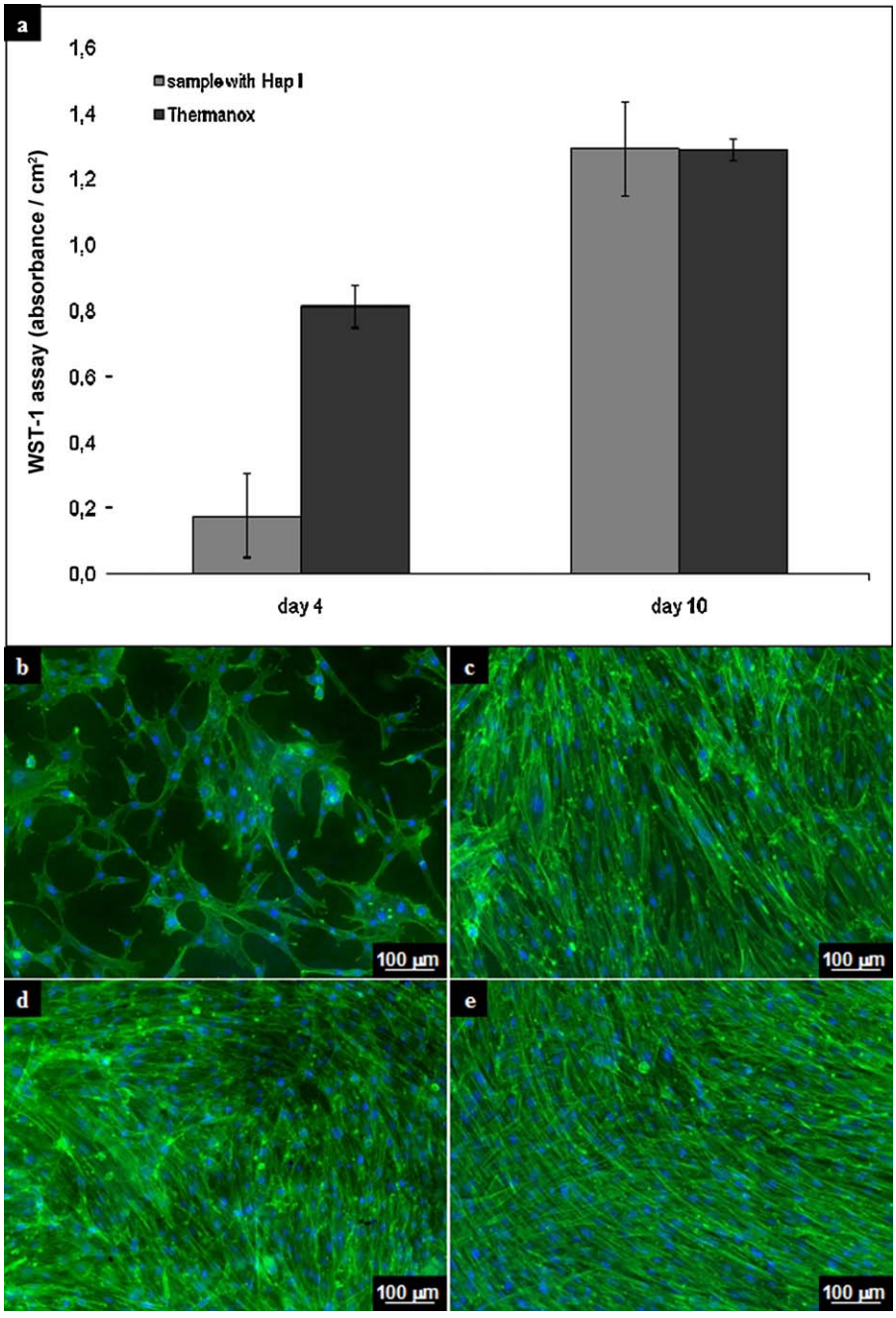

Fig. 5. Results from *in vitro* tests on wollastonite–hydroxyapatite composite containing HAp I and Thermanox: (a) WST-1 assay (normalised on surface area); (b–e) immunofluorescence staining (optical microscopy images of human osteoblasts): incubation for 4 days (b: composite; c: Thermanox) and 10 days (d: composite; e: Thermanox).

preceramic polymer when embedding HAp I powders instead of HAp C.

In Fig. 4c the internal positive (on the left side) and negative (on the right side) slices of selected HAp C (45% PMMA) cross-sections sample were compared. From the observation of the negative one it was possible to reproduce and visualize the pores interconnectivity.[32] In order to quantify the foam structure interconnectivity, a 'shrink-wrap' process was performed on the 3D foams reconstructions. As an example, Fig. 4d shows the interconnectivity percentage vs minimum connection size for HAp C (45% PMMA) sample. Considering that an opening between two pores can be considered an interconnection only when it is larger than a certain size, the interconnectivity value strongly depends on the defined minimum sizes. From the acquired data, it resulted that more than 97% of the pores were connected to their outside environment through openings of at least 52 μm (Fig. 4d). A remarkable decrement of the interconnectivity with increasing the minimum connection size was detected, in agreement with the trends observed by Shi et al. for nanocomposite scaffolds.[20] In details, according to data presented in Fig. 4d, the interconnectivity decreased from 97% for 52 μm minimum connection size to 12% for 312 μm.

Preliminary *in vitro* cell tests, with human osteoblasts, performed on wollastonite–hydroxyapatite composites prepared from HAp I filler, showed that cell growth and proliferation took place on material surface indicating that the composites are non-toxic. Although cell viability was higher on Thermanox on day 4, no significant differences in proliferation of the osteoblasts were found on day 10 (Fig. 5a).

The spreading and shape of cells on the samples were visualized at 4 and 10 days after seeding using AlexaFluor® 488 Phalloidin. On HAp I flattened and spread cells were visible, but also some spherical cells could be observed. In contrast, on Thermanox the surface was fully covered with flattened and spread cells (Fig. 5b and c). After 10 days cultivation, the surface of both materials, sample with HAp I and Thermanox, was fully covered with bone cells which formed multiple layers of well-flattened and spread cells. The actin cytoskeleton of the osteoblasts on HAp I was partially diffusely distributed and partially organized in stress fibres. On Thermanox the actin filaments were pronounced in stress fibres along the long axis of the cell (Fig. 5d and e).

As a final test, the samples were soaked for 7 days in CCM, in the absence of cells. EDX analysis (not reported here for the sake of brevity) on particulates found on composite surfaces, after 7 days, revealed the presence of Ca, P, Si, Na and Cl, and this could be associated to the formation of a calcium–phosphate layer on the ceramic substrate, indicative of the bioactivity of the materials.

Although very preliminary, *in vitro* tests with cells demonstrate that there were not toxic substances in the material and no toxic substance developed upon manufacturing. The formation of a calcium–phosphate layer reveals the potential of filled silicones to fabricate biocompatible and bioactive materials for bone tissue engineering. This was expected, since the wollastonite–hydroxyapatite coupling was inspired, as reported above, by well-established bioactive glass–ceramics; however, it should be noted that with the present approach of filled silicones the desired phase balance is achievable without glass melting and controlled crystallization, at very low temperature, thus configuring a much simplified processing cycle, with the fundamental additional advantage of the easy shaping of polymers.

The similarity of phase distribution between composites with HAp C and those with HAp I, despite differences in densification (e.g. porosity of struts in foamed samples), makes the biological tests quite reliable for composites with both types of fillers. Further biological tests, however, are undoubtedly needed, especially for comparing the behaviour of HAp nano- and micro-powders (samples from HAp C and HAp I compared with samples from HAp M) and will be the object of future work.

4. Conclusions

- We may conclude that $CaCO_3$, in the form of nano-sized particles, was proven to be an effective active filler for a silicone resin in order to form wollastonite; nano-sized powders led to a superior crystallinity and phase purity.
- Hydroxyapatite powders, although not completely inert when embedded in a mixture comprising silicone resin and carbonate active filler (the overall reactions are probably complex and need further investigations), were effective in leading to the formation of wollastonite–hydroxyapatite composites, exploiting the shaping possibilities given by the preceramic polymer.
- Mixtures of silicone resin, nano-$CaCO_3$ and (micro- or nano)-HAp were successfully shaped into open-celled foams, that could be used as scaffolds.
- The suitability of the produced cellular composites to applications in bone replacement and restoration was confirmed by both morphological analysis (also employing advanced micro-tomography imaging) and preliminary biological tests, consisting of biocompatibility and bioactivity assays.

Acknowledgements

E. Bernardo and P. Colombo thank Ms Chiara Bergo for the experimental assistance, Dr. Paola Palmero (Politecnico di Torino, Turin, Italy) and Dr. Giovanni Baldi (CeRiCol, Vinci, Firenze, Italy) for gently supplying HAp M and HAp C powders, respectively. E. Bernardo, P. Colombo, L. Treccani and K. Rezwan acknowledge the financial support of Italy–Germany bilateral research program “Vigoni”.

References

1. Greil P. *Polymer derived engineering ceramics*. *Adv Eng Mater* 2000;**6**:339–48.
2. Colombo P, Mera G, Riedel R, Sorarù GD. *Polymer-derived-ceramics: 40 years of research and innovation in advanced ceramics*. *J Am Ceram Soc* 2010;**93**:1805–37.
3. Bernardo E, Colombo P, Pippel E, Woltersdorf J, Novel mullite synthesis based on alumina nanoparticles a preceramic polymer. *J Am Ceram Soc* 2006;**89**:1577–83.
4. Griggio F, Bernardo E, Colombo P, Messing GL. *Kinetic studies of mullite synthesis from alumina nanoparticles and a preceramic polymer*. *J Am Ceram Soc* 2008;**91**:2529–33.
5. Parcianello G, Bernardo E, Colombo P. *Mullite/zirconia nano-composites from a preceramic polymer and nano-sized fillers*. *J Am Ceram Soc* 2011;**94**:1357–62.
6. Bernardo E, Colombo P, Hampshire S. *SiAlON-based ceramics from filled preceramic polymers*. *J Am Ceram Soc* 2006;**89**:3839–42.
7. Bernardo E, Colombo P, Hampshire S. *Advanced ceramics from preceramic polymers and nano-fillers*. *J Eur Ceram Soc* 2009;**29**:843–9.
8. Long LH, Chen LD, Chang J. *Low temperature fabrication and characterizations of* β-$CaSiO_3$ *ceramics*. *Ceram Int* 2006;**32**:457–60.
9. Batalova GV, Drogin VN, Vlasov AS, Belyakov AV, Lebedeva ED, Osipchik VS. *Conditions of shaping ceramics with a polyorganosiloxane bond*. *Glass Ceram* 1980;**37**:86–8.
10. Paszkievicz C, Gumuła T, Podporska J, Błażewicz M. *Structure and bioactivity of new polysiloxane-derived materials for orthopedic applications*. *J Mol Struct* 2006:176–81, 792–3.
11. Bernardo E, Tomasella E, Colombo P. *Development of multiphase bioceramics from a filler-containing preceramic polymer*. *Ceram Int* 2009;**35**:1415–21.
12. Schwarz KB, Rowcliffe DJ. *Modeling density contributions in preceramic polymer/ceramic powder systems*. *J Am Ceram Soc* 1986;**69**:C106–8.
13. Kokubo T. *Bioactive glass ceramics: properties and applications*. *Biomaterials* 1991;**12**:155–63.
14. Hench LL, Day DE, Höland W, Rheinberger VM. *Glass and medicine*. *Int J Appl Glass Sci* 2010;**1**:104–17.

15. Cacciotti I, Bianco A, Lombardi M, Montanaro L. *Mg-substituted hydroxyapatite nanopowders: synthesis, thermal stability and sintering behaviour*. *J Eur Ceram Soc* 2009;**29**:2969–78.
16. Bianco A, Cacciotti I, Lombardi M, Montanaro L, Gusmano G. *Thermal stability and sintering behaviour of hydroxyapatite nanopowders*. *J Therm Anal Calorim* 2007;**88**:237–43.
17. Bianco A, Cacciotti I, Lombardi M, Montanaro L. *Si-substituted hydroxyapatite nanopowders: synthesis, thermal stability and sinterability*. *Mater Res Bull* 2009;**44**:345–54.
18. Colombo P, Bernardo E. *Macro- and micro-cellular porous ceramics from preceramic polymers*. *Compos Sci Technol* 2003;**63**:2353–9.
19. Colombo P, Bernardo E, Biasetto L. *Novel microcellular ceramics from a silicone resin*. *J Am Ceram Soc* 2004;**87**:152–4.
20. Shi X, Sitharaman B, Pham QP, Liang F, Wu K, Edward Billups W, Wilson LJ, Mikos AG. *Fabrication of porous ultra-short single-walled carbon nanotube nanocomposite scaffolds for bone tissue engineering*. *Biomaterials* 2007;**28**:4078–90.
21. http://www.ing.unitn.it/∼maud/.
22. Chan CM, Wu JS, Li JX, Cheung YK. *Polypropylene/calcium carbonate nanocomposites*. *Polymer* 2002;**43**:2981–92.
23. Mishra S, Shimpi NG. *Mechanical and flame-retarding properties of styrene–butadiene rubber filled with nano-$CaCO_3$ as a filler and linseed oil as an extender*. *J Appl Polym Sci* 2005;**98**:2563–71.
24. Carter DR, Hayes WC. *Bone compressive strength: the influence of density and strain rate*. *Science* 1976;**104**:1174–6.
25. Prasher R, Song D, Wang J, Phelan P. *Measurements of nanofluid viscosity and its implications for thermal applications*. *Appl Phys Lett* 2006;**89**:133103–8.
26. Boccaccini AR. *On the viscosity of glass composites containing rigid inclusions*. *Mater Lett* 1998;**34**:285–9.
27. Gibson LJ, Ashby MF. Cellular solids structure and properties. 2nd ed. Cambridge UK: Cambridge University Press; 1999.
28. Deligianni DD, Katsala ND, Koutsoukos PG, Missirlis YF. *Effect of surface roughness of hydroxyapatite on human bone marrow cell adhesion, proliferation, differentiation and detachment strength*. *Biomaterials* 2001;**22**:87–96.
29. Vitale-Brovarone C, Verné E, Robiglio L, Appendino P, Bassi F, Martinasso G, Muzio G, Canuto R. *Development of glass–ceramic scaffolds for bone tissue engineering: characterisation, proliferation of human osteoblasts and nodule formation*. *Acta Biomater* 2007;**3**:199–208.
30. Dorozhkin SV. *Medical application of calcium orthophosphate bioceramics*. *BIO* 2011;**1**:1–51, @CCAAS.
31. Sanchez-Sálcedo S, Arcos D, Vallet-Regí M. *Upgrading calcium phosphate scaffolds for tissue engineering applications*. *Key Eng Mater* 2008;**377**:19–42.
32. Stauber M, Muller R. *Micro-computed tomography: a method for the non-destructive evaluation of the threedimensional structure of biological specimens*. *Methods Mol Biol* 2008;**455**:273–92.